

## Article

# A Study on Magnetization Yoke Design for Post-Assembly Magnetization Performance Improvement of a Spoke-Type Permanent Magnet Synchronous Motor

Min-Jae Jeong <sup>1</sup>, Kang-Been Lee <sup>2</sup> , Si-Woo Song <sup>3</sup>, Seung-Heon Lee <sup>4</sup> and Won-Ho Kim <sup>1,\*</sup> 

<sup>1</sup> Department of Electrical Engineering, Gachon University, Seongnam 13120, Republic of Korea; wjdalswo12@gachon.ac.kr

<sup>2</sup> Department of Electrical and Computer Engineering, Michigan State University, East Lansing, MI 48824, USA; leekangb@msu.edu

<sup>3</sup> Department of Electrical Engineering, Hanyang University, Seoul 04763, Republic of Korea; thdtldn93@hanyang.ac.kr

<sup>4</sup> Department of Next Generation Energy System Convergence, Gachon University, Seongnam 13120, Republic of Korea; dltdmdgjs153@gachon.ac.kr

\* Correspondence: wh15@gachon.ac.kr

**Abstract:** Permanent magnet synchronous motors (PMSMs) are highly affected by magnetization, which determines the magnetization level in the permanent magnet (PM). There are three main magnetization methods: single-unit, stator coil, and post-assembly magnetization. Post-assembly magnetization is widely used in PMSM mass production due to its ability to achieve high magnetization performance using a separate magnetizing yoke. However, spoke-type PMSMs with ferrite PMs face challenges when using the post-assembly method. The structural configuration of two magnets located radially hampers effective magnetized field transmission to the rotor's interior due to the narrow space between the magnets. Maximizing the magnetization rate becomes crucial, but the limited space in the spoke-type structure complicates this. This paper addresses the issue and analyzes factors influencing post-assembly magnetization characteristics. A novel yoke structure is proposed, reducing the distance between the coil and magnet, leading to more efficient magnetization. The parametric and performance comparative analysis shows an impressive 17.1%<sub>p</sub> increase in magnetization rate with the proposed yoke structure compared to the existing yoke. This outcome contributed to a solution for enhancing the magnetization performance of spoke-type ferrite PMSMs.

**Keywords:** ferrite magnet; magnetization yoke; post-assembly magnetization; spoke-type PMSM



**Citation:** Jeong, M.-J.; Lee, K.-B.; Song, S.-W.; Lee, S.-H.; Kim, W.-H. A Study on Magnetization Yoke Design for Post-Assembly Magnetization Performance Improvement of a Spoke-Type Permanent Magnet Synchronous Motor. *Machines* **2023**, *11*, 850. <https://doi.org/10.3390/machines11090850>

Academic Editors: Yawei Wang and Tianjie Zou

Received: 20 July 2023

Revised: 9 August 2023

Accepted: 18 August 2023

Published: 22 August 2023



**Copyright:** © 2023 by the authors. Licensee MDPI, Basel, Switzerland. This article is an open access article distributed under the terms and conditions of the Creative Commons Attribution (CC BY) license (<https://creativecommons.org/licenses/by/4.0/>).

## 1. Introduction

Recently, there has been a growing focus on achieving high efficiency in motors, driven by the rise in minimum efficiency requirements and environmental concerns. Consequently, there has been an increased interest in PMSMs. Specifically, PMs belonging to the rare earth series offer the advantages of enhanced power and motor miniaturization owing to their high energy density [1–4]. However, due to limited reserves of rare earth materials, their availability is restricted and comes at a high cost. These challenges have prompted active research on switch reluctance motors and synchronous reluctance motors that do not rely on rare earth PMs. Nonetheless, these alternative motor types encounter difficulties, such as lower power density, vibrations, and noise issues [5–10].

To address these challenges, extensive research has been undertaken on electric motors utilizing ferrite PMs, which are cost-effective and have abundant reserves. While ferrite PMs exhibit lower energy density than rare earth PMs, this drawback can be mitigated by implementing a magnetic flux concentration structure. The magnetic flux concentration structure arranges PMs in a radial direction, facing each other. This configuration results in a higher air gap magnetic flux density, as the cross-sectional area of the PM is significantly

larger than that of the air gap. Furthermore, the radial arrangement of the PMs enables a greater number of magnets to be accommodated within the rotor space [11–15]. Consequently, this approach enables the attainment of over 80% performance compared to rare earth motors, offering a promising solution to the rare earth scarcity issue.

However, one major limitation of spoke-type motors that has been identified is the challenge of magnetization after assembly. PM magnetization methods can generally be categorized into three types: single-unit magnetization, magnetization with stator coils, called in situ magnetization, and yoke magnetization, named post-assembly magnetization [16]. In the case of the single-unit magnetization method, excellent magnetization performance is achieved by directly applying a magnetization magnetic field to the PM. However, when assembling the magnetized PM onto the rotor, difficulties arise due to the attraction and repulsion of magnets, leading to challenges in the assembly process. Additionally, assembly tolerances may occur due to iron powder adsorbed on the magnet's surface.

On the other hand, in situ magnetization involves assembling the PMs onto the rotor and then magnetizing them after combining them with the stator. This method effectively resolves the problems encountered with single-piece magnetization, as magnetization occurs after the PMs are assembled. However, when dealing with PMs possessing high coercive force, the magnetization process may give rise to issues like winding deformation and insulation breakdown. Furthermore, effective magnetic field transmission to the PM becomes challenging when the number of poles and teeth is not properly matched.

Another magnetization approach is post-assembly magnetization, where a PM is inserted into a magnetization yoke and magnetized [17,18]. This method involves selecting and designing a yoke structure and winding specifications specifically tailored for magnetization, thereby addressing the limitations associated with the magnetization with stator coil. Additionally, since the PM undergoes magnetization during assembly onto the rotor, it resolves the problems encountered with the single-unit magnetization of the PM. Therefore, PMSMs generally adopt the magnetization method after assembly, utilizing a magnetization yoke to meet mass production and magnetization performance requirements.

Therefore, permanent magnet motors that must be mass-produced use post-assembly magnetization using a magnetizing yoke. Although PMSMs have been built using post-assembly magnetization, applying the post-assembly magnetization method to spoke-type PMSMs is difficult. A maximum magnetic field should be applied to the PM to increase the magnetization rate. However, due to the spoke-type structure in which the PMs are arranged radially, the magnetized field does not reach the PM inside the rotor. Spoke-type PMSM is a motor to reduce the dependence on rare earths, so it is essential to find a solution to this problem.

In order to solve this problem, a study was conducted to improve the post-assembly magnetization performance by utilizing the split-multiple magnetization method. This method greatly improved the permanent magnet magnetization performance by concentrating the magnetizing field on a specific permanent magnet. However, the lifetime of the yoke is short due to the increase in the number of magnetizations. Also, the irreversible demagnetization of the magnetized magnet must be considered during the magnetization process [19]. Therefore, in this paper, a study was conducted to improve the magnetization performance with a single magnetizer rather than a split multi-magnetizer. Existing magnetization studies do not consider coil fixers. And magnetizer manufacturers also do not produce them considering this. However, if the magnetizing yoke is designed considering this, the post-assembly magnetization performance can be greatly improved. Therefore, in this paper, a new magnetic yoke shape design was proposed.

## 2. Specification and FEM of the Target Motor

### 2.1. Specification of Target Motor

The target spoke-type ferrite PMSM applied to the conveyor belt is selected, as shown in Figure 1. The arrow on the permanent magnet in Figure 1 indicates the magnetization direction of the permanent magnet. The motor features eight poles and 12 slots, operating

in a three-phase configuration. It is designed to deliver a torque of 7.5 Nm, with a rated rotation speed of 1800 RPM. The stator possesses an outer diameter of 155 mm, and an air gap of 0.5 mm is performed between the stator and rotor. The stack length is 90 mm. Both the stator and rotor are constructed using the material 35PN230. Finally, the magnet is selected as ferrite, K30iH. A comprehensive summary of the specifications of the motor can be found in Table 1, providing further details.

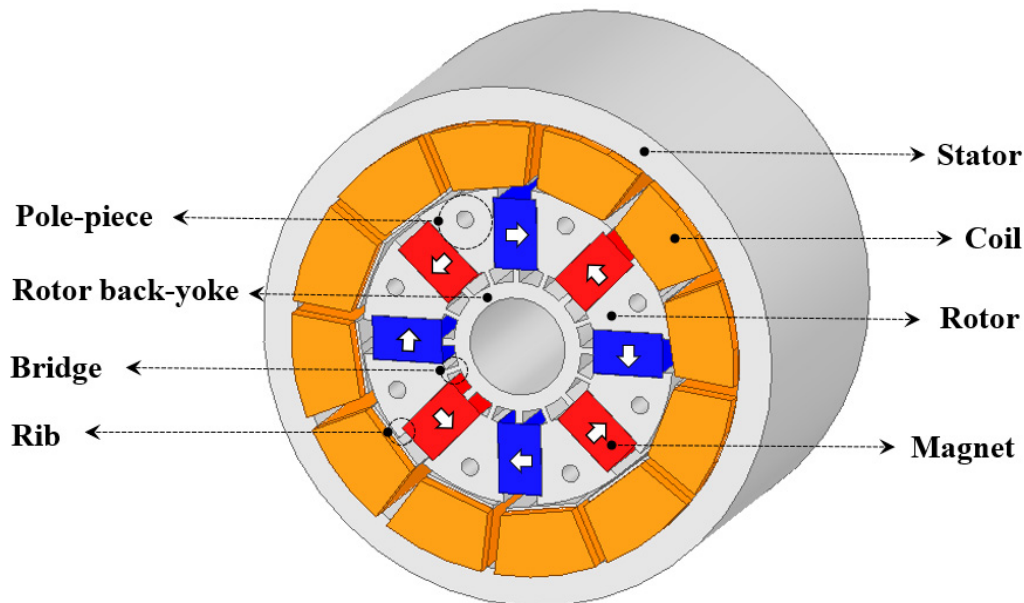


Figure 1. Description picture of target motor.

Table 1. Specification of target motor.

	Item	Value	Unit
Specification	Poles/Slots	8/12	-
	Phase	3	-
	Voltage	380	V
	Torque	8.5	Nm
	Rotating speed	1800	RPM
	Number of turns	74	-
Size	Outer/Inner diameter of stator	155/95.4	mm
	Outer/Inner diameter of rotor	94.4/29	mm
	Length of airgap	0.5	mm
	Stack length	90	mm
Material	Stator	35PN230	-
	Rotor	35PN230	-
	Coil	Copper	-
	Magnet	Ferrite (K30iH)	-
	Shaft	S45C	-

## 2.2. FEM of Target Motor

Section 2.2 presents the result of a simulation of the no-load and load characteristics of the target motor. Figure 2 shows the analysis result of the no-load back EMF of phases a, b, and c of the target motor. It has a value of 157 V<sub>rms</sub>. Figure 3 shows the cogging torque analysis results, and the peak-to-peak value is shown as being 548 m Nm. Due to the nature of the spoke-type motor using additional reluctance torque, the cogging torque is large. Figure 4 shows the torque analysis result at a current of 3.3 Arms. It has an average

torque of 8.5 Nm required by the conveyor belt. Figure 5 shows the harmonic analysis results. Looking at Figure 5, the 5th and 7th harmonics appear relatively high. Figure 6 is the torque–speed curve of the target motor. The red line is the magnetic torque, and the black line is the reluctance torque. Additionally, the blue line is the total torque of magnetic torque and reluctance torque. The target motor for the conveyor belt in this paper must satisfy a torque of 8 Nm or more at 1800 RPM. As shown in Figure 6, at the 1800 RPM speed point, the reluctance torque is about 2.4 Nm, and the magnetic torque is 6.2 Nm, which adds up to 8.6 Nm. Therefore, the target torque of 8 Nm at 1800 rpm is satisfied.

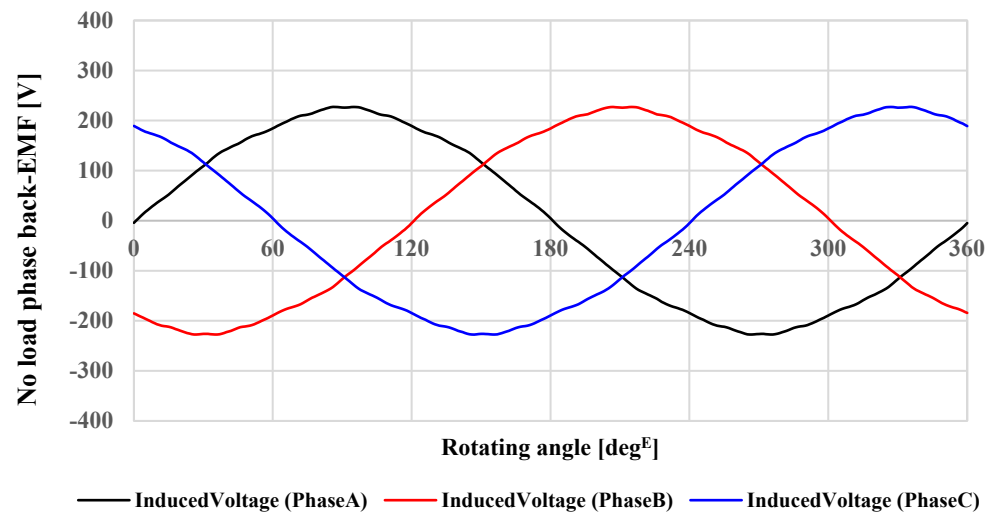


Figure 2. No-load phase back-EMF of target motor.

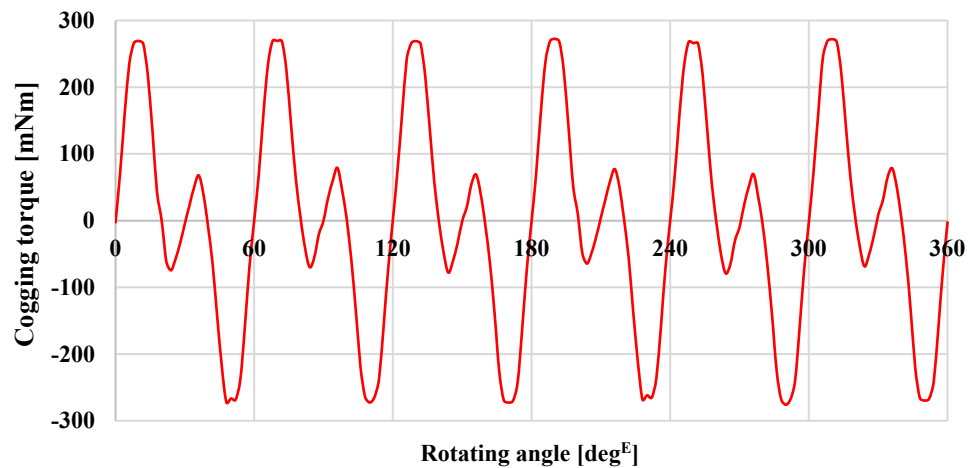


Figure 3. Cogging torque of target motor.

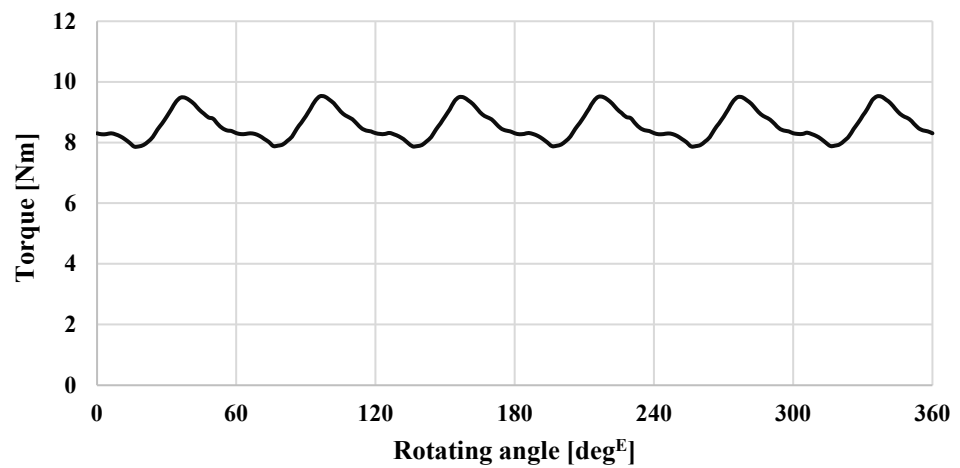


Figure 4. Load torque of target motor.

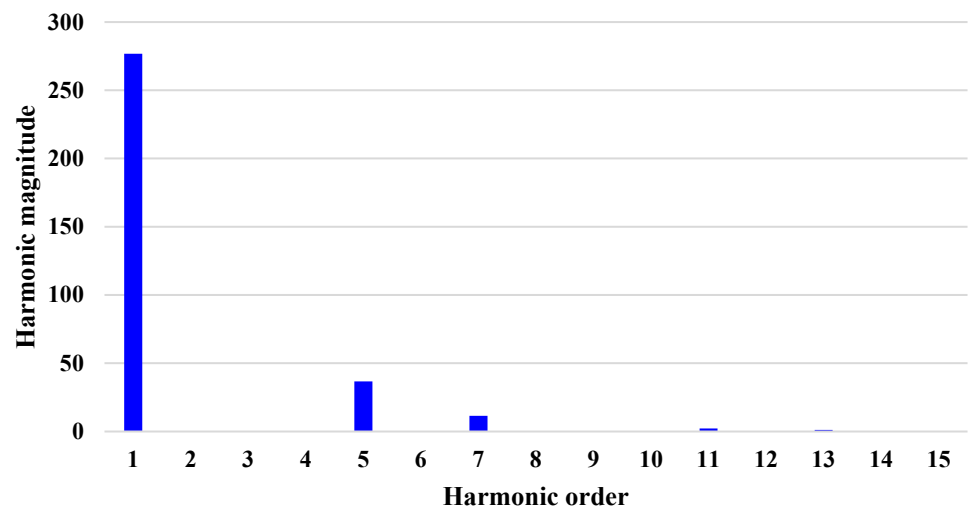


Figure 5. Harmonic analysis of target motor.

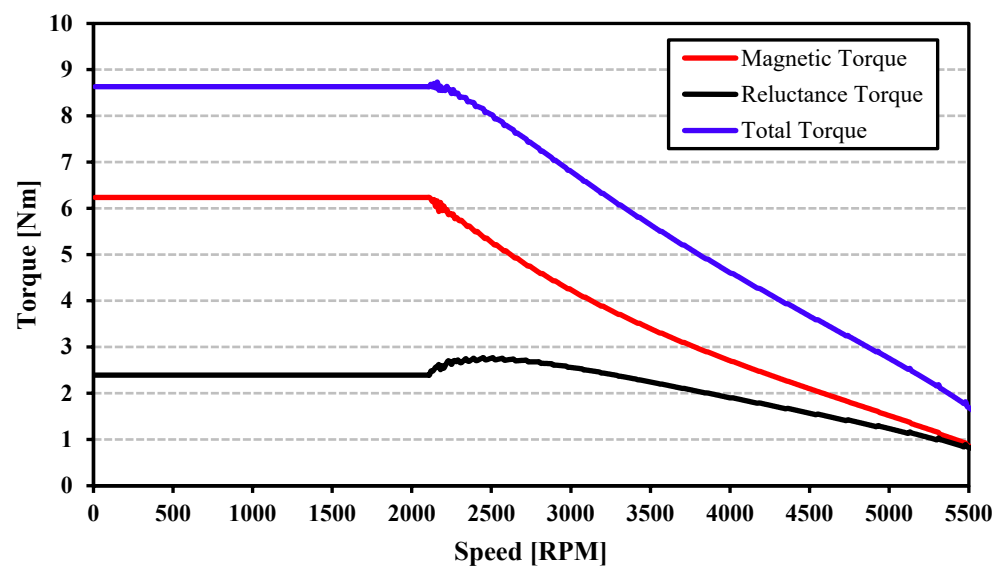


Figure 6. T-N curve of target motor.

### 3. Magnetizing Principle and Method of Permanent Magnet

#### 3.1. Principle of Permanent Magnet Magnetization

In the atomic model of a ferromagnetic substance, the source of the magnetic field is the magnetic dipole moment  $m$ . If there are  $n$  magnetic dipoles per unit volume, there are  $n\Delta V$  total magnetic dipole moments in the volume  $\Delta V$ . Since each magnetic dipole moment value is different, the vector sum of all magnetic dipole moments in this volume is given by Equation (1).

$$m_{total} = \sum_{i=1}^{n\Delta V} m_i \quad (1)$$

Magnetization  $M$  is a new quantity representing the magnetic dipole moment per unit volume. It is expressed by Equation (2) and the unit is [A/m] like  $H$ .

$$M = \frac{1}{\Delta V} \sum_{i=1}^{n\Delta V} m_i \quad (2)$$

Magnetization  $M$  is caused by a bound current. Additionally, since it has the same physical quantity as the strength of the magnetic field, Ampere's circuital law can be applied. The bound current included in the integration path  $dl$  can be expressed as Equation (3). Additionally,  $I_b$  can be expressed by Equation (4).

$$dI_b = nI_b dS \cdot dl = M \cdot dl \quad (3)$$

$$I_b = \oint M \cdot dl = I_T \quad (4)$$

Therefore, Ampere's circuital law in free space is given by the sum of the conductor current and the bound current. This is expressed by Equation (5).

$$\oint \frac{B}{\mu_0} \cdot dl = I_T \quad (5)$$

$I_T$  in Equation (5) is the sum of  $I$  and  $I_b$ . Additionally,  $I$  is the current due to free electrons in the conductor. Equation (6) is obtained by deriving the equation of conductor current based on Equation (5).

$$I = I_T - I_b = \oint \left( \frac{B}{\mu_0} - M \right) \cdot dl \quad (6)$$

By applying  $B$  and  $M$ , the magnetic field strength by conductor current can be defined. Additionally, this is expressed in Equation (7).

$$H = \frac{B}{\mu_0} - M \quad (7)$$

At this time, it becomes  $B = \mu_0 H$  in the free space where the magnetization is zero, and the magnetic flux density  $B$  in the material where the magnetization exists is expressed by Equation (8).

$$B = \mu_0 (H + M) \quad (8)$$

As shown in Figure 7, magnetization  $M$  becomes saturated when a sufficiently large external magnetic field is applied. Therefore, when an external magnetic field is applied until it is saturated, magnetization  $M$  is approximately proportional to the magnitude of the external magnetic field. This proportional constant is defined as the magnetic susceptibility  $x_m$ . Therefore, magnetization  $M$  is expressed as Equation (9).

$$M = x_m H \quad (9)$$

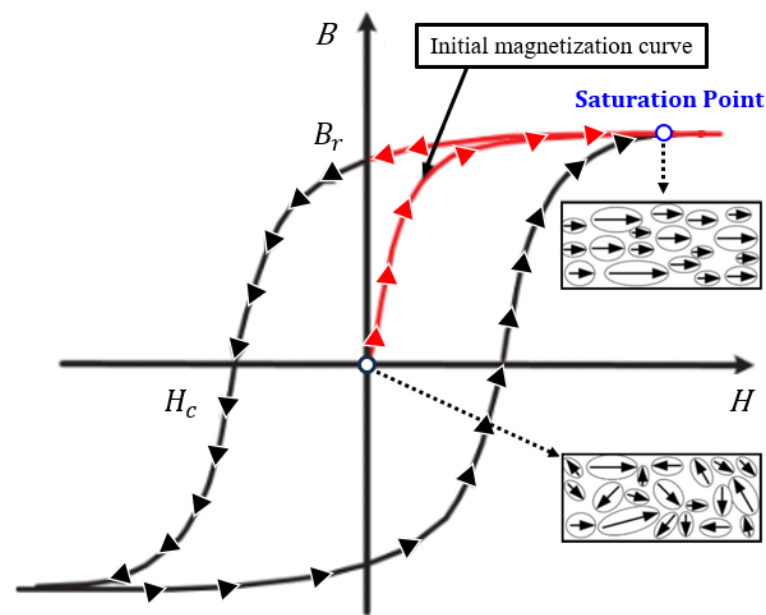


Figure 7. Initial and hysteresis curve of PM.

Equation (10) is obtained by substituting Equation (9) into Equation (8).

$$B = \mu_0(1 + x_m)H = \mu_0\mu_r H \quad (10)$$

$\mu_r$  is an integer defined as the relative magnetic permeability. Relative magnetic permeability varies depending on the material, and its value has a great influence on the characteristics of electrical devices. In ferromagnetic materials, pure iron has a relative magnetic permeability close to 10,000. Therefore, if the same magnetic field is applied to pure iron and air, pure iron generates 1000 times more magnetic flux than air. The relative magnetic permeability of electrical steel sheet, which is an important material used in electrical equipment, is about 3000, and the saturation magnetic flux density is about 1.5–1.8 [T]. Additionally, air, permanent magnets, conductors, and insulators have a relative magnetic permeability of 1.

In a ferromagnetic material, the arrangement of atomic magnets is random in the absence of an external magnetic field. Consequently, the magnetic forces produced by individual atomic magnets counteract each other, preventing the emission of an external magnetic force. However, when enough external magnetic field is applied, the magnetic forces originating from each atomic magnet align parallel to the external field. Consequently, the cumulative magnetic forces no longer cancel each other out, releasing a magnetic force in the direction influenced by the external magnetic field. This process of aligning the magnetic poles of atomic magnets in a single direction by subjecting the magnetic material to a strong external magnetic field is referred to as magnetization.

Figure 7 illustrates a hysteresis curve depicting a PM's magnetization process to provide a more comprehensive explanation. In Figure 7, the black line is the overall hysteresis curve and the red line is the initial magnetization curve. The figure elucidates how the magnetic flux density ( $B$ ) increases along the initial magnetization curve as the magnetic field intensifies ( $H$ ). There is a substantial increase in magnetic flux density relative to the change in the magnetic field in the initial magnetization process. However, once the saturation point is reached, the change becomes negligible. This occurs because the alignment of atomic magnets reaches completion at the saturation point, rendering additional magnetic force unnecessary.

The magnetic flux density persists when the magnetic field is applied up to the saturation point and subsequently reduced to zero. This is known as the residual magnetic flux density. Moreover, materials that retain magnetic flux density even in the absence of

an external magnetic field are classified as PMs. Based on the underlying magnetization mechanism elucidated above, it becomes evident that a magnetic field must be applied for an unmagnetized PM to function as a magnetic flux source until the saturation point is reached.

### 3.2. PM Magnetization Methods

Magnetizing PMs is crucial to serve as the primary magnetic flux source in PMSMs. PM magnetization methods can be categorized into three types: single-unit magnetization, magnetization through the stator coil, and post-assembly magnetization. Figure 8 visually represents these methods, where (a) corresponds to the single-unit magnetization method, (b) demonstrates the magnetization method through the stator coil, and (c) depicts the post-assembly magnetization.

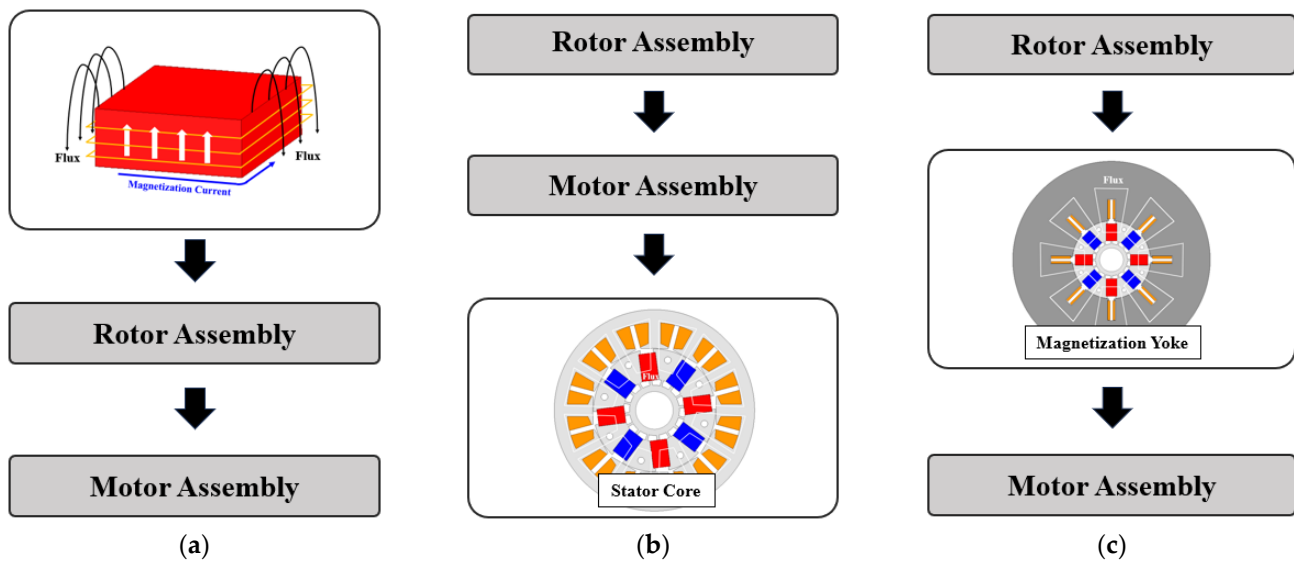


**Figure 8.** Method of permanent magnetization: (a) single-unit magnetization; (b) in situ magnetization; (c) post-assembly magnetization.

- The single-unit magnetization method involves magnetizing one or more magnets by directly applying a magnetic field, as shown in Figure 8a. In this method, the magnetization process occurs before the magnets are assembled onto the rotor, enabling the magnetic field to be fully applied to the PM. This results in excellent magnetization characteristics. However, the drawback of this method is the challenges encountered during the assembly process due to the attraction and repulsion of magnets. Moreover, iron powder adhered to the magnet's surface can lead to manufacturing issues such as assembly tolerance. Consequently, the single-unit magnetization method is not well-suited for mass production processes.
- The in situ magnetization method involves magnetizing a PM after it has been assembled onto a rotor and combined with a stator. A schematic diagram illustrating the in situ magnetization process is presented in Figure 8b. By magnetizing the PMs after assembly, this method effectively addresses the limitations encountered in the single-unit magnetization approach. However, challenges may arise when dealing with PMs with high coercive force, such as winding deformation and insulation breakdown during the magnetization process. Furthermore, ensuring the effective transmission of a magnetic field to a PM becomes difficult when the number of poles and teeth do not align properly.
- Finally, the post-assembly magnetization method involves magnetizing the PM using a separate magnetizing yoke. With the PM inserted, the rotor is coupled to the magnetizing yoke, magnetized, and then assembled into the motor. Figure 8c illustrates the process of post-assembly magnetization. This method addresses challenges in in situ

magnetization, such as mismatch between the number of poles and teeth, winding deformation, and dielectric breakdown. These issues can be effectively resolved by selecting and designing an appropriate yoke structure and winding specifications for magnetization. Moreover, since the PM is magnetized while being assembled onto the rotor, this method overcomes the limitations of single-unit magnetization. As a result, PMSMs generally adopt a magnetization method after assembly, utilizing a magnetization yoke to simultaneously achieve high mass productivity and magnetization performance.

#### 4. Analysis of Post-Assembly Magnetization

The yoke structure for magnetization is presented in Figure 9. The structure, including the coil support structure, where the structure fixes the coils in the magnetization yoke, pole piece, where the partial stator between two adjacent magnets, and teeth of the yoke are defined. The defined titles of the components will be used in the following sections.

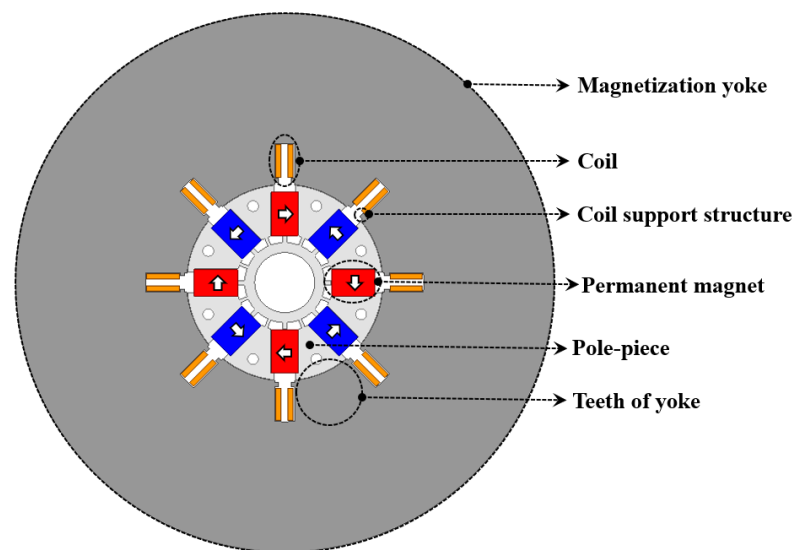


**Figure 9.** Description picture of magnetization yoke.

##### 4.1. Circuit Analysis

A magnetic equivalent circuit was developed to analyze the magnetization characteristics of the post-assembly magnetization method, as depicted in Figure 10. In the post-assembly magnetization approach, using ferromagnetic material with high permeability in the magnetizing yoke facilitates efficient magnetic field transmission to the PM, as the magnetic flux tends to flow towards areas with higher permeability. Initially, the magnetic resistances of  $R_t$ ,  $R_y$ , and  $R_p$  are nearly zero. However, during the magnetization process, these resistances deviate from near-zero values. This is due to the requirement of a significantly large magnetic field for magnetizing the PM. The immense magnetizing field causes saturation of the yoke and pole piece, rendering them similar to air permeability. Consequently,  $R_t$ ,  $R_y$ , and  $R_p$  become equivalent to the magnetic resistance  $R_g$  of air.

##### 4.2. Finite-Element Analysis

In this paper, two-dimensional FEA was conducted, and commercial finite element analysis Maxwell software 2020 R2 version was used. The 2D FEM is used to calculate the magnetic field in the machine section  $x, y$  plane. The Maxwell equation applied to the air gap, iron core, and permanent magnet regions is presented in Equation (11).

$$\nabla \cdot (v \nabla A) - \sigma \frac{\partial A}{\partial t} = v \mu_0 \left( \frac{\partial M_x}{\partial y} - \frac{\partial M_y}{\partial x} \right) \quad (11)$$

$\nu$  equals the equivalent relativity in the permanent magnet. Additionally, the left formulation term exists in a permanent magnet. The relativity  $\nu$  of the material is a function of magnetic flux density so that the formula can calculate saturated iron cores [20,21].

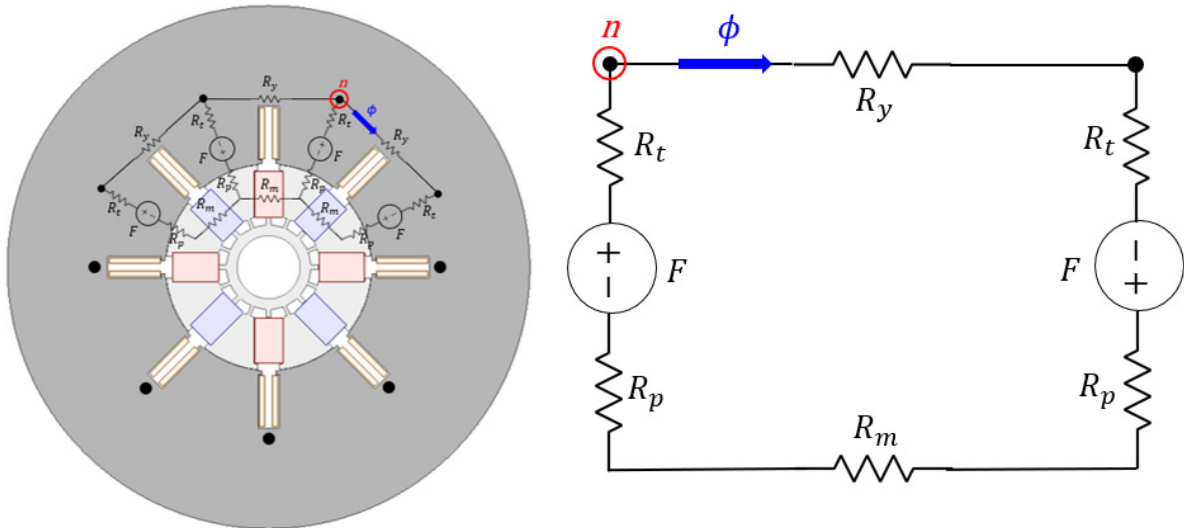


Figure 10. Magnetic equivalent circuit of magnetizer.

4.3. Magnetic Field Analysis of Post-Assembly Magnetization

The magnetic flux density analysis result shows the magnetizing yoke and pole piece saturation when post-assembly magnetization is conducted, as shown in Figure 11. Since it is generally assumed that the magnetic flux density of a ferromagnetic material exceeds 2T, it is saturated, so the range of magnetic flux density was plotted by limiting it up to 2T, and the area where the magnetic flux density was more than 2T was marked in red as evidence of saturation. Since the magnetizing yoke and pole piece are saturated during magnetization and have large magnetic resistance, it is necessary to investigate the change in magnetization performance according to the winding arrangement.

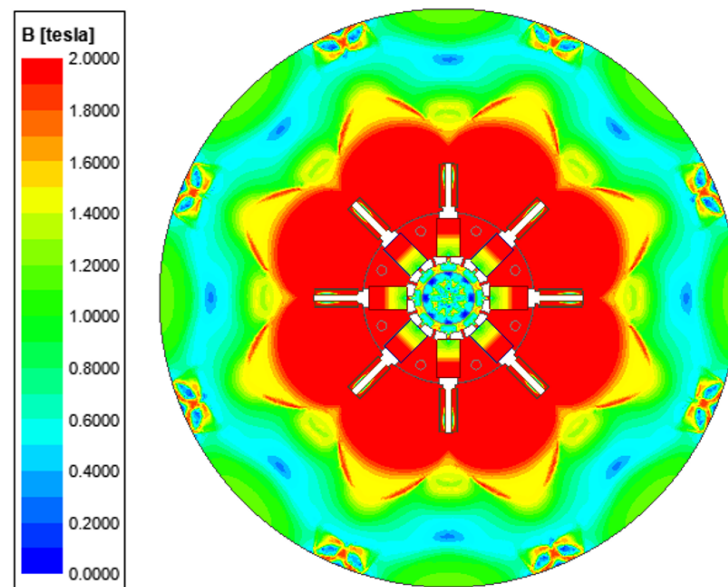


Figure 11. Saturation analysis of magnetizing yoke.

4.4. Magnetic Field Analysis of Post-Assembly Magnetization

Figure 12 shows the 1st and 2nd quadrants of the permanent magnet hysteresis curve of ferrite K30iH used in the post-assembly magnetization analysis in this paper. As can be

seen from Figure 7 above, all magnetic moments must be aligned in order to magnetize a permanent magnet. The criterion for determining magnetization is the point at which the relative permeability becomes equal to the permeability of air. Looking at the hysteresis curve of ferrite K30iH, the relative permeability becomes equal to the permeability of air at the point of 7.1 kOe. The conversion of 7.1 kOe to MKS results in a value of 565 kA/m. Therefore, whether the permanent magnet is magnetized is determined based on the point where the magnetic field applied to the permanent magnet exceeds 565 kA/m.

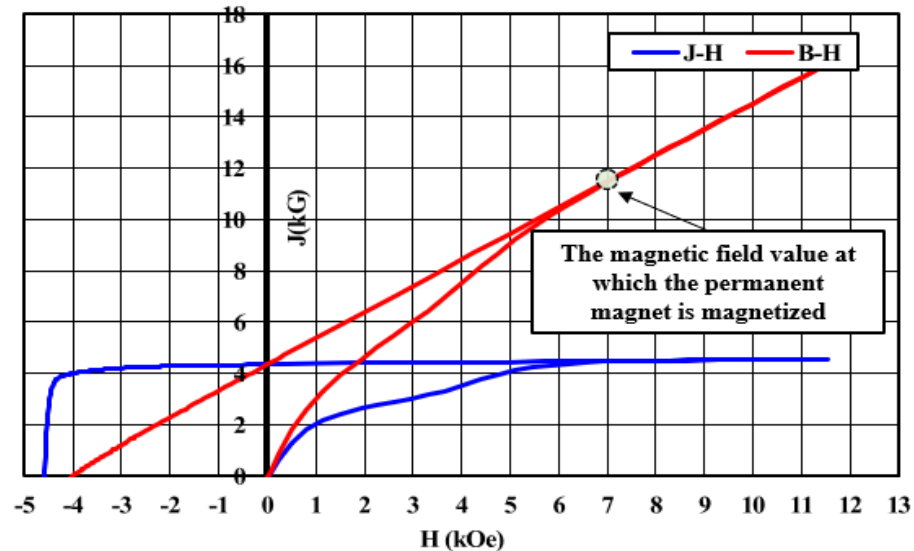


Figure 12. Hysteresis curve of ferrite permanent magnet (K30iH).

#### 4.5. Effect of Winding Position on Post-Assembly Magnetization

In most motor designs, the stator teeth are intentionally prevented from becoming oversaturated. This precautionary measure is taken because when the stator reaches saturation, the torque value relative to the applied winding current diminishes, leading to a decline in efficiency. Consequently, most of the magnetic flux generated by the windings follows a path along the stator and pole-piece, irrespective of the winding position. However, unlike motor design principles, a substantial magnetomotive force is necessitated during the magnetization of a PM to ensure complete saturation of the teeth in both the magnetizing yoke and the pole-piece. Even if a magnetic material with high magnetic permeability is employed to enhance the effective transfer of magnetic flux to the PM, it exhibits non-magnetic properties due to saturation.

A parametric analysis was carried out to investigate the influence of winding arrangement on magnetization performance, as shown in Figure 13. The objective was to examine the impact of different winding positions on the characteristics of post-assembly magnetization. The windings were systematically repositioned at 10 mm intervals (0–30 mm) from the outer diameter of the pole-piece. During the parametric analysis, the number of turns and current values were kept constant to solely evaluate the effects of winding arrangement.

The findings from the parametric analysis are presented in Figure 14. The magnetized region of the PM is depicted in red, while the blue region represents an unmagnetized area. It is evident that as the winding position moves further from the outer diameter of the pole-piece, the unmagnetized area expands. This phenomenon occurs because the saturation of the magnetizing yoke and pole-piece leads to a significant increase in magnetic resistance, thereby shortening the path of the magnetic flux generated within the winding. As a result, a considerable portion of the magnetic flux produced by the magnetizing yoke does not reach the pole-piece but instead forms around the winding. Consequently, when the winding and the PM are distanced, the PM fails to receive an adequate magnetizing field. The analysis outcomes emphasize the importance of considering the influence of winding arrangement when designing the magnetizing yoke in the case of post-assembly magnetization.

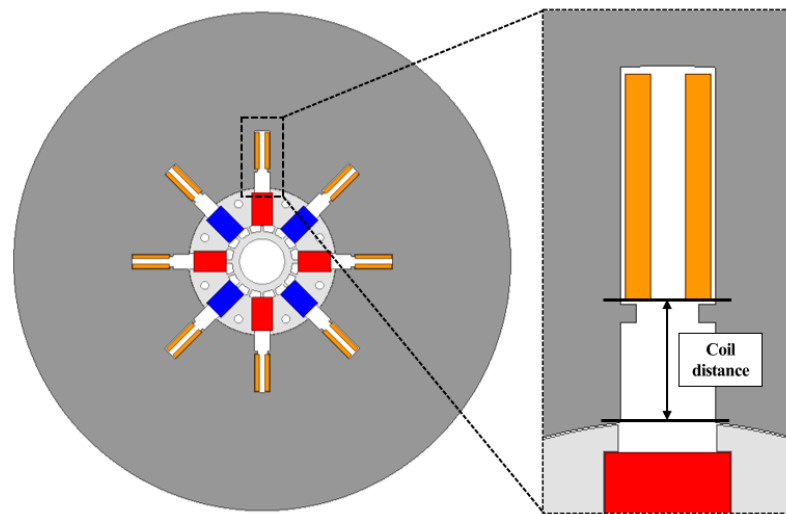


**Figure 13.** Example of magnetizing yoke coil arrangement.

#### 4.6. Magnetic Flux Path Analysis

In order to validate the results obtained from the parametric analysis, a flux path analysis was conducted. The models considered in this analysis were based on different separation distances between the pole piece and winding, specifically 0 mm, 10 mm, 20 mm, and 30 mm, as depicted in Figure 15a–d, respectively.

Consistent with the initial estimates, the analysis confirmed that the magnetic resistance of the yoke and pole piece was significantly high, resulting in the magnetic flux generated from the winding predominantly flowing around the winding rather than along the yoke and pole piece. As illustrated in Figure 15a, when the distance between the winding and the PM was short, a major portion of the magnetic flux traversed through the PM.

Conversely, in the model with a larger distance between the PM and the winding, as shown in Figure 15b–d, most of the magnetic flux passed through the yoke rather than the PM. These observations indicate that models receiving greater magnetizing flux directed towards the PM exhibit superior magnetization characteristics. Consequently, the location of the coil emerges as a significant factor influencing the magnetization performance of the yoke.

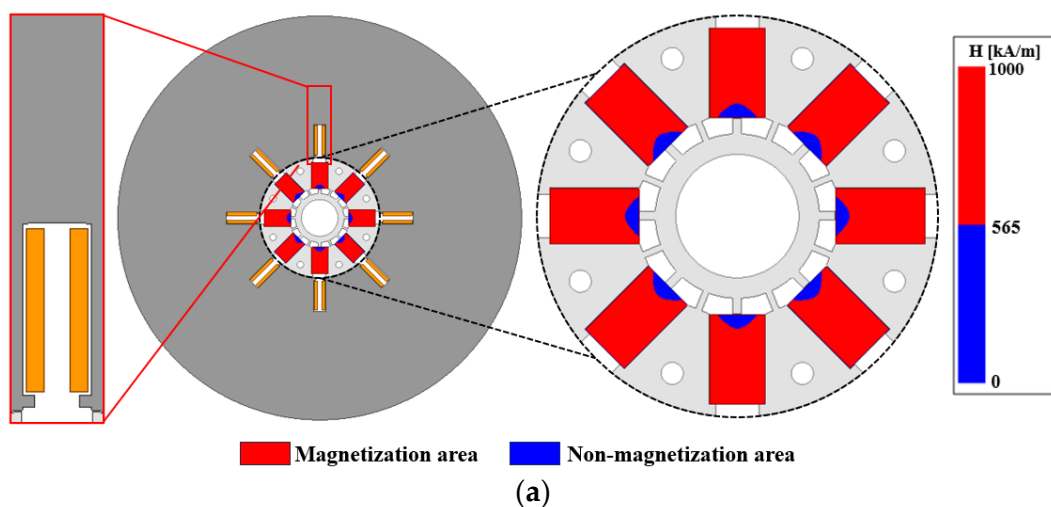


**Figure 14.** Cont.

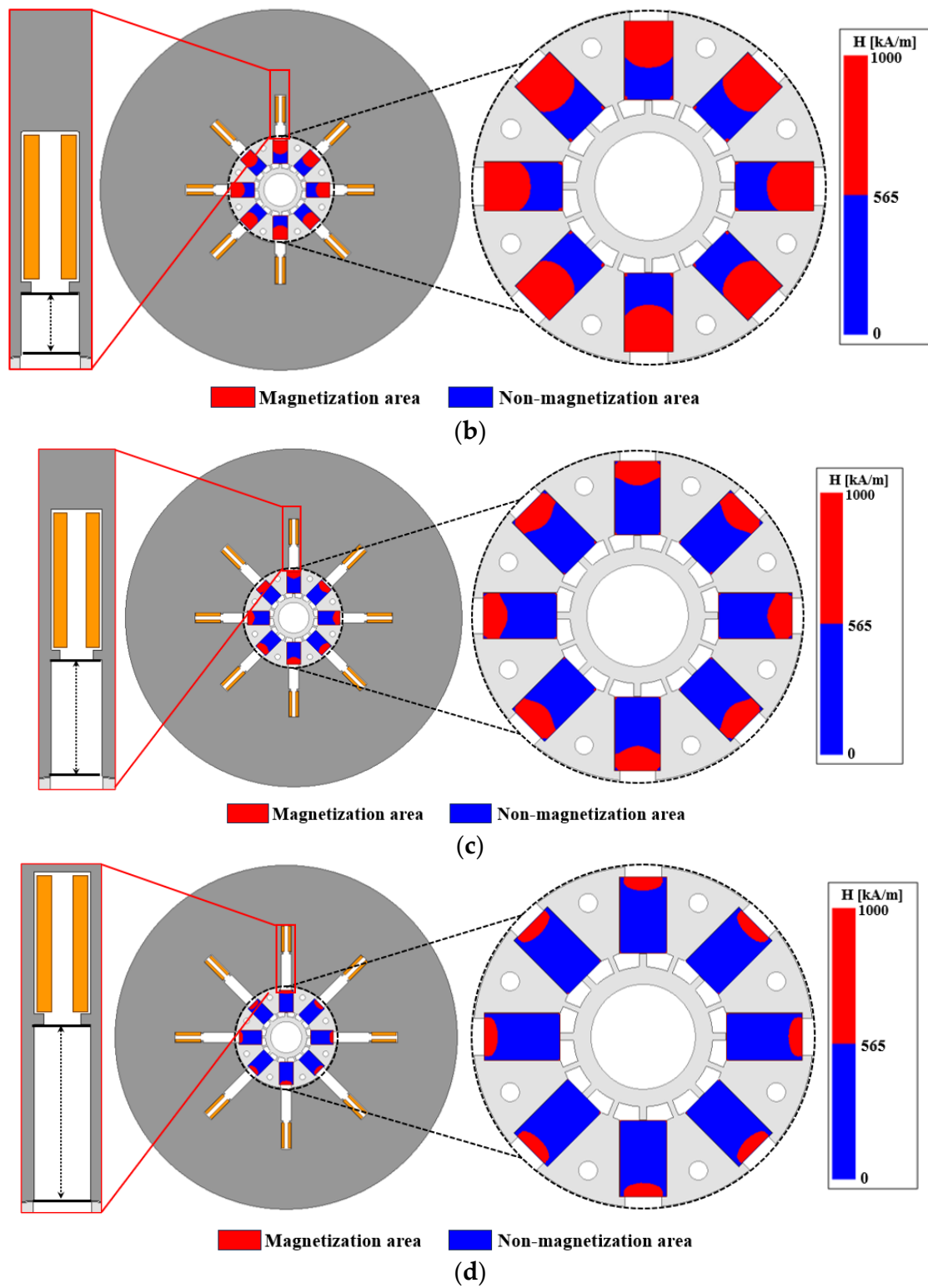


Figure 14. Post-assembly magnetization: (a) distance 0 mm; (b) distance 10 mm; (c) distance 20 mm; (d) distance 30 mm.

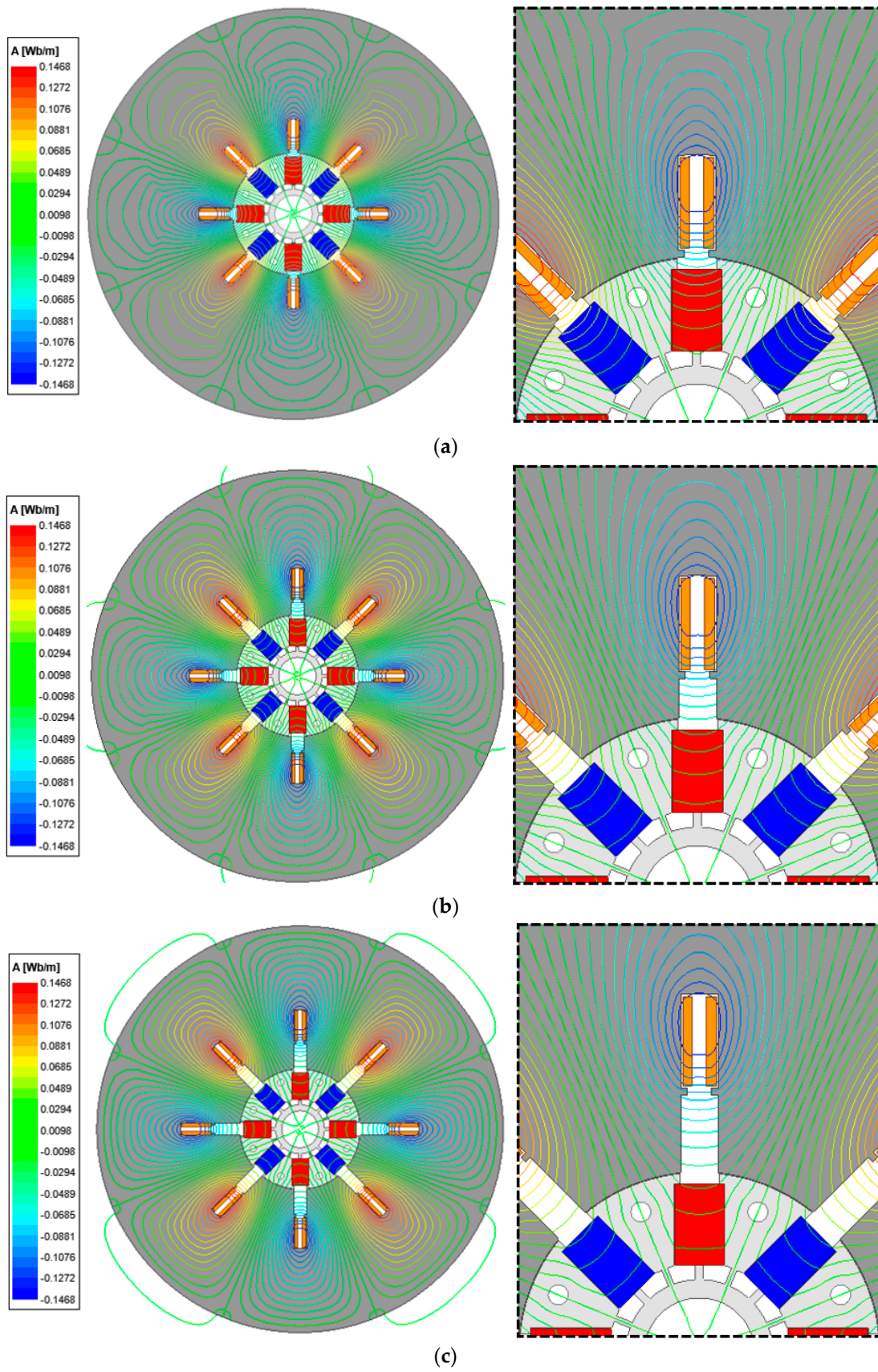
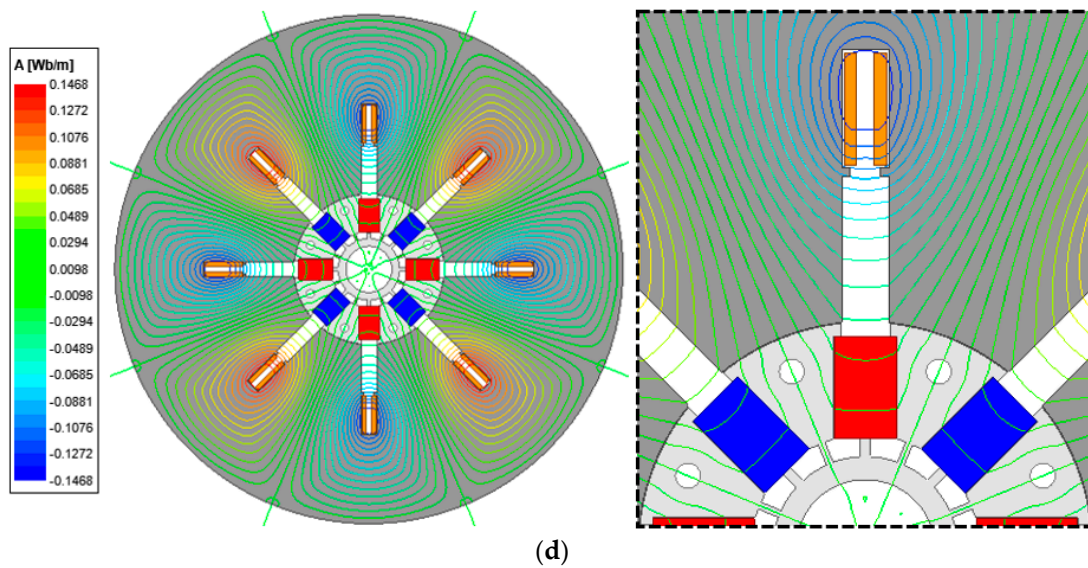


Figure 15. Cont.



**Figure 15.** Flux-line analysis: (a) distance 0 mm; (b) distance 10 mm; (c) distance 20 mm; (d) distance 30 mm.

### 5. Yoke Design for Improved Post-Assembly Magnetization Performance

Table 2 summarizes the existing yoke specifications based on the target motor's specifications. The coils have a diameter of 2.6 mm and a total of six turns. The yoke, made of S20C material, has an inner diameter of 95.4 mm, an outer diameter of 155 mm, and an air gap of 0.22 mm. The yoke structure was parameterized to achieve an optimal yoke structure design, as depicted in Figure 16. Figure 16 shows the basic model sets  $A_l$  to 0.2 mm,  $S_w$  and  $S_h$  to 1.5 mm and 2.2 mm, respectively. Considering that the coil wire has a diameter of  $2.6\Phi$  and six turns,  $C_w$  is 2.6 mm, and  $C_h$  is 23.4 mm. Finally,  $R_w$  and  $R_h$  are set to 1.5 mm and 3.2 mm, respectively.

**Table 2.** Specification of target motor.

	Item	Value	Unit
Specification	Diameter of coil	2.6	mm
	Number of turns	6	-
Size	Inner diameter of yoke	95.4	mm
	Outer diameter of yoke	155	mm
	Length of air gap	0.2	mm
Material	Magnetization yoke	S20C	-
	Coil	Copper	-

The coil support structure plays a crucial role in securing the coil within the yoke during the winding process, preventing it from dislodging. Furthermore, during magnetization, it effectively mitigates coil deviation resulting from the forces between the coils induced by high currents. The rib serves a dual purpose of preventing the scattering of permanent magnets and providing a pathway for the flow of leaked magnetic flux. Therefore, having a shorter lip length in motors with high flux concentration, denoted as  $R_w$ , is preferable as it positively impacts motor performance by concentrating the flux. Typically, these motors have a minimum  $R_w$  length that is sufficient to securely hold the permanent magnet in place. On the other hand, the thickness of the rib, denoted as  $R_h$ , significantly influences both irreversible demagnetization and magnetization performance. Reducing  $R_h$  can improve magnetization performance by decreasing the distance between the permanent magnet and the coil wire. However, it also increases the risk of irreversible demagnetization during load operation. Considering the trade-off relationship between

magnetization performance and demagnetization, the optimal length of  $R_h$  should be carefully designed to achieve a balance between magnetization performance and irreversible demagnetization.

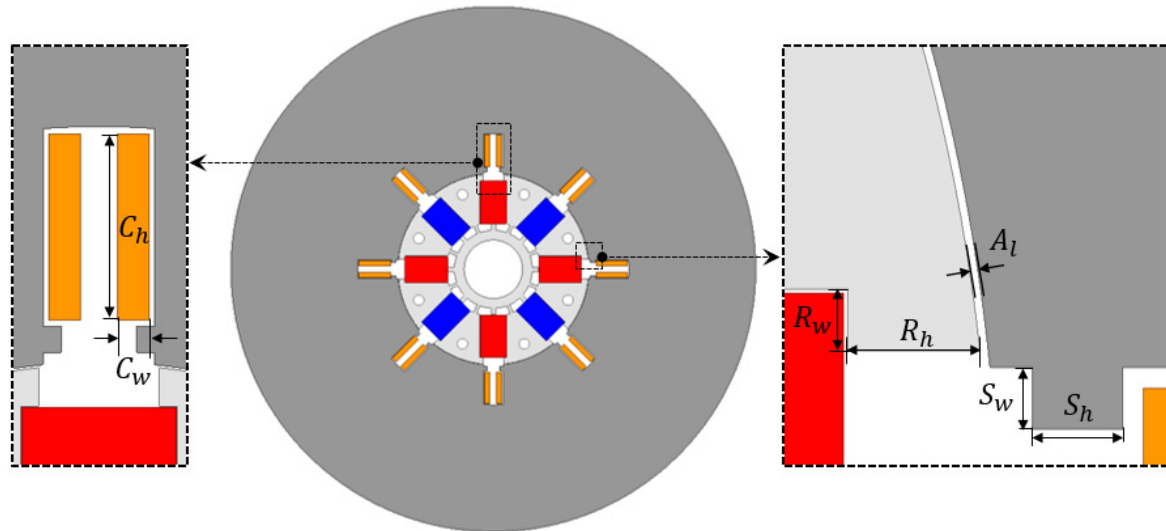


**Figure 16.** Basic model of magnetization yoke.

Based on the parametric analysis results and trade-off relationship, magnetization performance improvements can be achieved by reducing the coil distance, minimizing the rib thickness to reduce leakage flux, and ensuring a sufficient rib height to prevent irreversible demagnetization of the permanent magnet. A design proposal, illustrated in Figure 17, has been put forward to enhance magnetization performance without irreversible demagnetization. Unlike the existing magnetizing yoke, where the coil-supporting structure is located outside the rotor, the proposed magnetizing yoke is designed to minimize the coil distance by incorporating the yoke between the ribs.

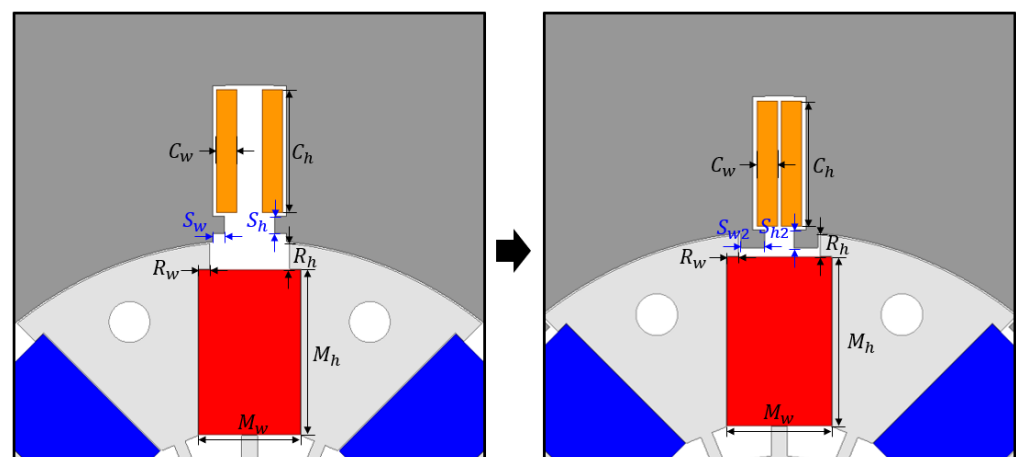


**Figure 17.** The proposed yoke model of magnetization yoke.

This design facilitates efficient transmission of the magnetic field generated by the coil to the permanent magnet. The height of the support coil structure,  $S_{h2}$ , is designed to be shorter than the rib length ( $R_h$ ), while the width of the support coil structure,  $S_{w2}$ , is wide enough to accommodate the coil wire diameter,  $C_w$ .  $S_{h2}$  is set at 2.2 mm and  $S_{w2}$  at 3 mm to meet these requirements. Additionally, the magnetization performance is enhanced by filling the empty space at the top of the permanent magnet in the spoke-type PMSM, minimizing demagnetization.

## 6. FEA Analysis

### 6.1. Post-Assembly Magnetization 2D-Simulation

A two-dimensional finite element analysis (FEA) model was constructed to validate the proposed yoke. The magnetization specifications involved applying a voltage of 3500 V<sub>dc</sub> and a capacitance of 3000 μF to the coil, as outlined in Table 3. The applied voltage and current at the coil are presented in Figures 18 and 19. The peak currents of the basic and redesigned models are described as 11.6 kA and 11.7 kA.

**Table 3.** Magnetizer specifications and magnetizing current.

Model	Voltage	Capacitance	Peak Current
Basic model	3500 V <sub>dc</sub>	3000 μF	11.6 kA
Proposed model			11.7 kA

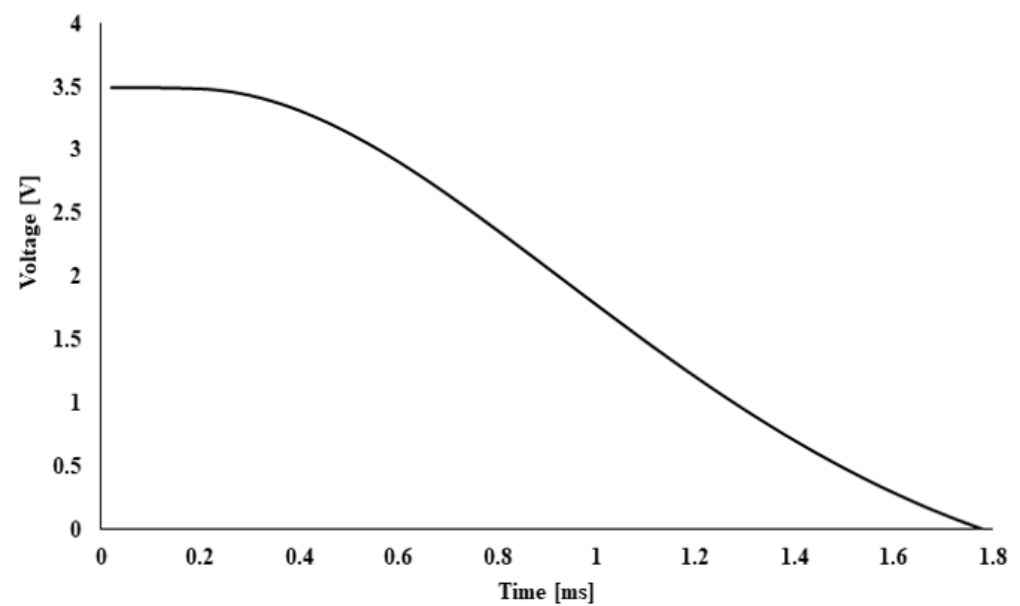


**Figure 18.** Applied voltage for post-assembly magnetization analysis.

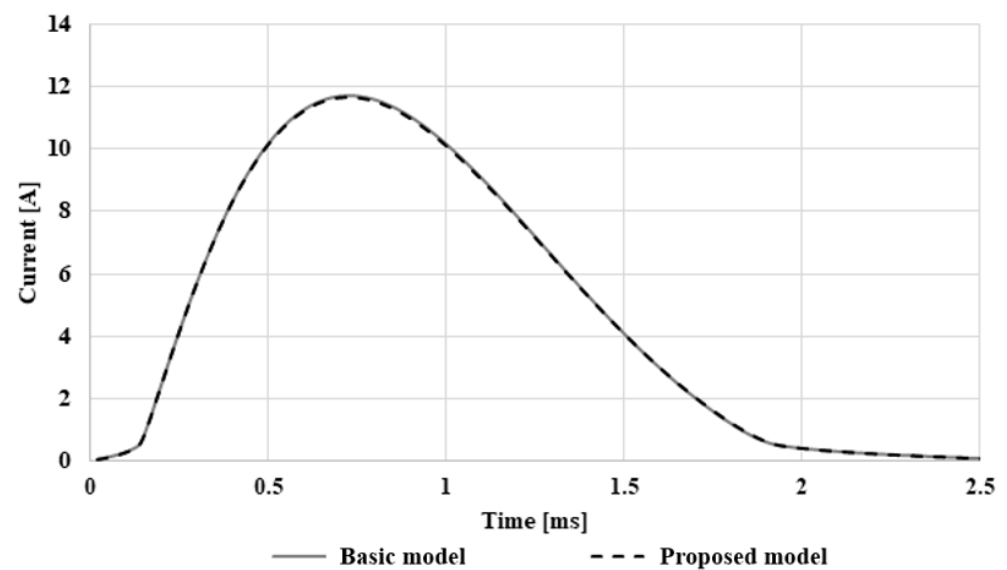


**Figure 19.** Applied current for post-assembly magnetization analysis.

In order to ensure a fair and accurate comparison of the impact on magnetization performance between the proposed yoke and other factors, the coil specifications were kept consistent. Specifically, the number of turns per tooth was set at six turns, and the wire diameter was 2.6 mm. This leads to the coil resistances at the basic and redesigned models, which are 0.15984 Ω and 0.15760 Ω at 50 °C. The resistance of the coil was evaluated for both the basic and the redesigned models, and the corresponding values are presented in Table 4.

**Table 4.** Specifications and resistance of coil.

Model	Number of Turns	Diameter of Coil	Resistance of Coil
Basic model	6	2.6φ	0.15984 Ω (50 °C)
Proposed model			0.15760 Ω (50 °C)

6.2. Performance Validation of the Proposed Magnetization Yoke

Figures 20 and 21 depict a comparison of magnetization performances between the basic and redesigned models, as obtained from the FEA results. The red-colored region represents the magnetized area, while the blue-colored region represents the unmagnetized area. It is evident from the figures that the redesigned model exhibits a wider magnetized area. This observation confirms the effectiveness of the redesigned model in transmitting the magnetized magnetic field to the permanent magnet.

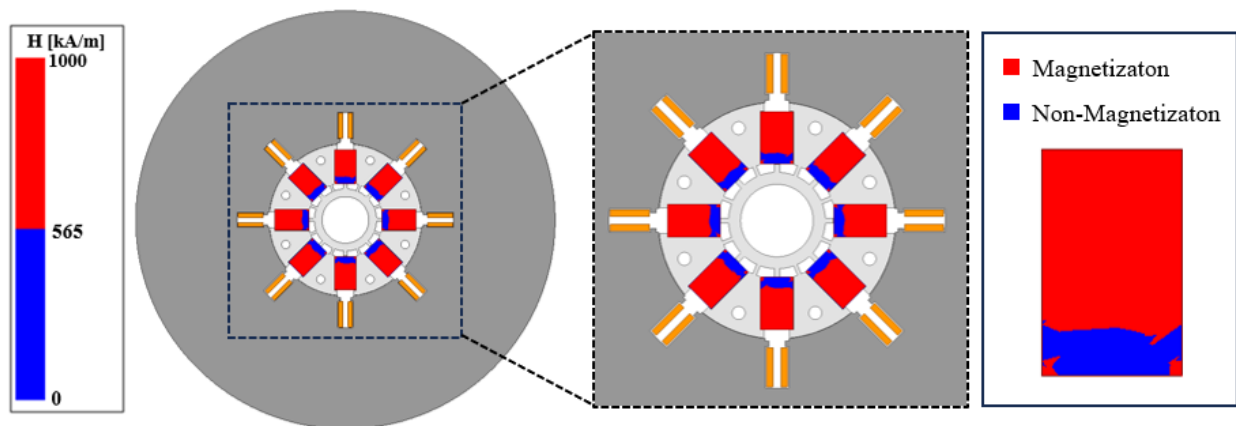


**Figure 20.** Post-assembly magnetization 2D-simulation results of the basic model.

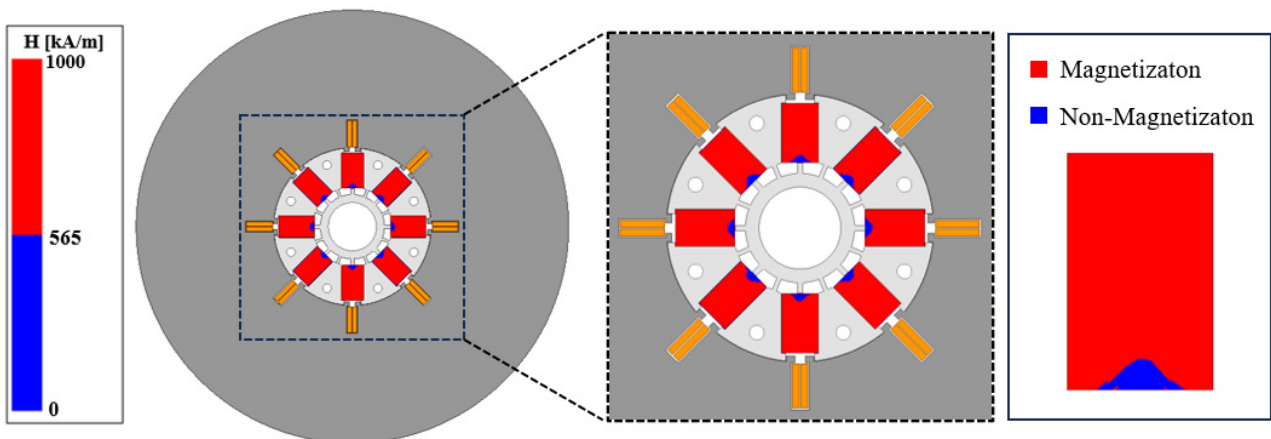


**Figure 21.** Post-assembly magnetization 2D-simulation results of the redesigned model.

### 6.3. Performance Comparison after Post-Assembly Magnetization

In order to perform an accurate comparison of magnetization performance between the three models, the full magnetization model, the existing basic yoke model, and the proposed yoke model, the no-load back electromotive forces (EMFs) were examined after magnetization. Table 5 presents the back EMF was presented as 140.4 V<sub>rms</sub> from the full magnetization model. Subsequently, for the basic model and the redesigned model, the EMFs were estimated to be 114.4 V<sub>rms</sub> and 135.3 V<sub>rms</sub>, respectively, as shown in Figure 22 by FEA.

**Table 5.** Magnetization ratio of PM.

Model	No-Load Phase Back EMF	Magnetization Ratio of Magnet
Master	140.4 V <sub>rms</sub>	Standard
Basic model	114.4 V <sub>rms</sub>	79.3%
Proposed model	135.3 V <sub>rms</sub>	96.4%

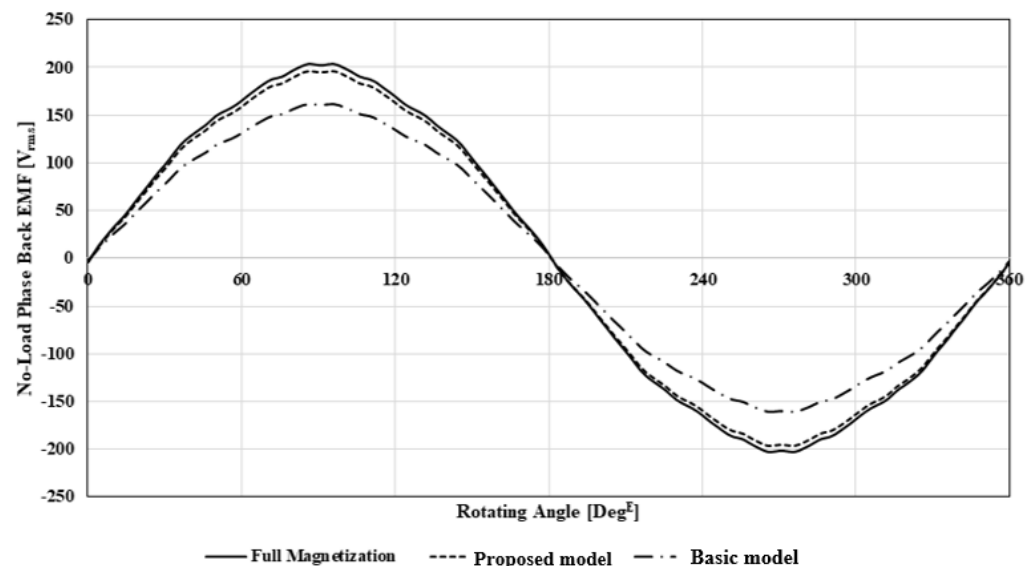


**Figure 22.** Comparison of no-load phase back-EMF for each model.

Converting these values into a PM magnetization rate, the basic model demonstrated a rate of 79.3%, whereas the redesigned model exhibited a rate of 96.4%. This signifies a significant increase of 17.1%<sub>p</sub> in the permanent magnet magnetization rate compared to the basic model when the redesigned yoke structure is used. Thus, the results provide empirical evidence for the positive impact of improving the magnetizing yoke on the permanent magnet magnetization rate.

## 7. Conclusions

This paper aimed to investigate and enhance the magnetization performance of spoke-type ferrite PMSMs after assembly. Ferrite PM is receiving more attention in the building of electric machines due to the limited market and skyrocketing cost of rare earth PMs. While post-assembly magnetization is commonly employed in PMSMs for efficient mass production and magnetization performance, its application to spoke-type PMSMs is challenging due to the unique structural characteristics of the rotor. This study analyzed the factors influencing magnetization performance and proposed a novel yoke structure to address ferrite PMs and post-assembly magnetization's advantages. The primary cause of deteriorated magnetization performance is the saturation of the yoke, which results in a shortened magnetic field path. Consequently, the magnetic field fails to penetrate the rotor interior, demagnetizing the permanent magnet. A new magnetizing yoke shape was

proposed to mitigate these challenges. With a parametric and performance comparative analysis, a significant improvement in the magnetization rate of the permanent magnet was achieved. It was validated that the redesigned model of the yoke produces a 17.1%<sub>p</sub> better magnetization rate compared to the existing basic model by FEA.

**Author Contributions:** Conceptualization, W.-H.K.; methodology, M.-J.J.; software, M.-J.J.; validation, S.-W.S.; formal analysis, S.-H.L.; investigation, M.-J.J.; resources, M.-J.J.; data curation, M.-J.J.; writing, original draft preparation, M.-J.J.; writing, review and editing, K.-B.L.; visualization, K.-B.L.; supervision, K.-B.L.; project administration, M.-J.J.; funding acquisition, W.-H.K. All authors have read and agreed to the published version of the manuscript.

**Funding:** This work was partly supported by the Korea Institute of Energy Technology Evaluation and Planning (KETEP) grant funded by the Korea government (MOTIE) (20214000000060, Department of Next Generation Energy System Convergence based-on Techno-Economics—STEP) and in part by the Gachon University Research Fund of 2020 under Grant GCU-202008450007.

**Data Availability Statement:** Not applicable.

**Conflicts of Interest:** The authors declare no conflict of interest.

## Nomenclature

$m$	magnetic moment
$B$	magnetic flux density, T
$B_r$	residual flux density, T
$\mu$	absolute permeability, H/m
$\mu_0$	permeability of vacuum
$\mu_r$	relative permeability
$M$	magnetization vector
$M_x$	$x$ components of the magnetization vector in the permanent magnet
$M_y$	$y$ components of the magnetization vector in the permanent magnet
$H$	magnetic field intensity, A/m
$x_m$	magnetic susceptibility
$R_t$	resistances of teeth
$R_y$	resistances of yoke
$R_p$	resistances of pole piece
$R_m$	resistances of magnet
$R_g$	resistances of air gap
$F$	magnetomotive force, A
$A$	axial component of magnetic vector potential
$\nu$	reluctivity of material in the permanent magnet
$\sigma$	conductivity, S/m
$C_w$	determined by the coil diameter
$C_h$	the product of the final number of turns and the coil diameter determines
$A_l$	Air gap between the magnetizing yoke and the rotor
$S_w$	width of the protrusion supporting the coil
$S_h$	length of the protrusion supporting the coil
$R_w$	width of the rib
$R_h$	length of the rib

## References

1. Tao, X.; Takemoto, M.; Tsunata, R.; Ogasawara, S. Novel rotor structure employing large flux barrier and disproportional airgap for enhancing efficiency of IPMSM adopting concentrated winding structure. *IEEE Access* **2022**, *11*, 2848–2862. [[CrossRef](#)]
2. Du, J.; Wang, X.; Lv, H. Optimization of magnet shape based on efficiency map of IPMSM for EVs. *IEEE Trans. Appl. Supercond.* **2016**, *26*, 609807. [[CrossRef](#)]
3. Hu, H.; Zhao, J.; Liu, X.; Chen, Z.; Gu, Z.; Sui, Y. Research on the torque ripple and scanning range of an arc-structure PMSM used for scanning system. *IEEE Trans. Magn.* **2014**, *50*, 8105504. [[CrossRef](#)]
4. Hwang, S.-W.; Chin, J.-W.; Lim, M.-S. Design process and verification of SPMSM for a wearable robot Considering thermal characteristics through LPTN. *IEEE/ASME Trans. Mechatron.* **2021**, *26*, 1033–1042. [[CrossRef](#)]

5. Chiba, A.; Kiyota, K.; Hoshi, N.; Takemoto, M.; Ogasawara, S. Development of a Rare-earth-free SR motor with high torque density for hybrid vehicles. *IEEE Trans. Energy Convers.* **2015**, *30*, 175–182. [[CrossRef](#)]
6. Yu, F.; Chen, H.; Yan, W.; Zhou, D.; Wang, X.; Gorbounov, Y.; Anuchin, A.; Demidova, G.; Korovkin, N.; Liudmila, S. Performance improvement for double-stator axial flux SRM using a new winding reconfigurable power converter. *IEEE Trans. Transp. Electrif.* **2023**, *9*, 3295–3307. [[CrossRef](#)]
7. Kim, K.-C.; Ahn, J.S.; Won, S.H.; Hong, J.-P.; Lee, J. A study on the optimal design of SynRM for the high torque and power factor. *IEEE Trans. Magn.* **2007**, *43*, 2543–2545. [[CrossRef](#)]
8. Niazi, P.; Toliyat, H.A.; Goodarzi, A. Robust maximum Torque per ampere (MTPA) control of PM-assisted SynRM for traction applications. *IEEE Trans. Veh. Technol.* **2007**, *56*, 1538–1545. [[CrossRef](#)]
9. Fereydoonian, M.; Lee, K.; Bobba, D.; Lee, W. Comparative analysis of wound-field flux-switching machines with different field and armature winding configurations. In Proceedings of the 2022 IEEE Transportation Electrification Conference & Expo (ITEC), Anaheim, CA, USA, 15–17 June 2022; pp. 1076–1081.
10. Fereydoonian, M.; Bobba, D.; Lee, W. Magnetic flux path and inductance analysis of flux-switching machines with different field and armature winding configurations. In Proceedings of the 2022 IEEE Energy Conversion Congress and Exposition (ECCE), Detroit, MI, USA, 9–13 October 2022; pp. 1–7.
11. Zhou, Y.; Yang, X. Analytical Method to Calculate Inductances of Spoke-Type Permanent-Magnet Synchronous Motors with Damping Bars. *IEEE Trans. Ind. Electron.* **2023**, *70*, 8254–8263. [[CrossRef](#)]
12. Kashif, M.; Singh, B. Solar PV-Fed Reverse Saliency Spoke-Type PMSM with Hybrid ANF-Based Self-Sensing for Water Pump System. *IEEE J. Emerg. Sel. Top. Power Electron.* **2022**, *10*, 3927–3939. [[CrossRef](#)]
13. Muthusamy, M.; Hendershot, J.; Pillay, P. Design of a Spoke Type PMSM with SMC Stator Core for Traction Applications. *IEEE Trans. Ind. Appl.* **2023**, *59*, 1418–1436. [[CrossRef](#)]
14. Lee, Y.-H.; Hsieh, M.F.; Chen, P.-H. A Novel Variable Flux Spoke Type Permanent Magnet Motor with Swiveling Magnetization for Electric Vehicles. *IEEE Access* **2022**, *10*, 62194–62209. [[CrossRef](#)]
15. Jung, J.-W.; Jung, D.-H.; Lee, J. A Study on the Design Method for Improving the Efficiency of Spoke-Type PMSM. *IEEE Trans. Magn.* **2023**, *59*, 8200205. [[CrossRef](#)]
16. Kim, K.-S.; Park, M.-R.; Kim, H.-J.; Chai, S.-H.; Hong, J.-P. Estimation of rotor type using ferrite magnet considering the magnetization Process. *IEEE Trans. Magn.* **2016**, *52*, 8101804. [[CrossRef](#)]
17. Hsieh, M.-F.; Hsu, Y.-C.; Dorrell, D.G. Design of large-power surface-mounted permanent-magnet motors using post assembly magnetization. *IEEE Trans. Ind. Electron.* **2010**, *57*, 3376–3384. [[CrossRef](#)]
18. Hsieh, M.-F.; Lien, Y.-M.; Dorrell, D.G. Post-assembly magnetization of rare-earth fractional-slot surface permanent-magnet machines using a two-shot method. *IEEE Trans. Ind. Appl.* **2011**, *47*, 2478–2486. [[CrossRef](#)]
19. Seol, H.-S.; Jeong, T.-C.; Jun, H.-W.; Lee, J.; Kang, D.-W. Design of 3-Times magnetizer and rotor of spoke-type PMSM considering post-assembly magnetization. *IEEE Trans. Magn.* **2017**, *53*, 8208005. [[CrossRef](#)]
20. Fu, W.N.; Zhou, P.; Lin, D.; Stanton, S.; Cendes, Z.J. Modeling of solid conductors in two-dimensional transient finite-element analysis and its application to electric machines. *IEEE Trans. Magn.* **2004**, *40*, 426–434. [[CrossRef](#)]
21. Fu, W.N.; Ho, S.L. Extension of the concept of windings in magnetic field electric circuit coupled finite element method. *IEEE Trans. Magn.* **2010**, *46*, 2119–2123. [[CrossRef](#)]

**Disclaimer/Publisher’s Note:** The statements, opinions and data contained in all publications are solely those of the individual author(s) and contributor(s) and not of MDPI and/or the editor(s). MDPI and/or the editor(s) disclaim responsibility for any injury to people or property resulting from any ideas, methods, instructions or products referred to in the content.